CRYO / 02 / 031
December, 13, 2002

Analysis of Electrical Coupling Parameters in Superconducting Cables

L. Bottura, M. Breschi[b], C. Rosso

[b] DIE, Department of Electrical Engineering, University of Bologna, Italy

Distribution: Internal

Presented: Workshop on Computation of Thermo-Hydraulic Transients in Superconductors, Karlsruhe, 15-18 September, 2002

Published: to appear in Cryogenics, 2003

Summary

The analysis of current distribution and redistribution in superconducting cables requires the knowledge of the electric coupling among strands, and in particular the interstrand resistance and inductance values. In practice both parameters can have wide variations in cables commonly used such as Rutherford cables for accelerators or Cable-in-Conduits for fusion and SMES magnets. In this paper we describe a model of a multi-stage twisted cable with arbitrary geometry that can be used to study the range of interstrand resistances and inductances that is associated with variations of geometry. These variations can be due to cabling or compaction effects. To describe the variations from the nominal geometry we have adopted a cable model that resembles to the physical process of cabling and compaction. The inductance calculation part of the model is validated by comparison to semi-analytical results, showing excellent accuracy and execution speed.

Introduction

Any analysis of current distribution and re-distribution in multi-strand superconducting cables (see for instance [1-6]) depends in last analysis on the assumptions made on the electrical characteristics of the cable. The main parameters that are of importance are in particular the strand longitudinal resistance, theinterstrand conductance and the strand self and mutual inductances. The strand longitudinal resistance depends on the V-I characteristics of the superconducting material and the associated stabilizer. This is typically one of the characteristics that can be well established through measurements on

single strands in various conditions. The interstrand conductance depends largely on strand coatings, surface conditions, cabling pattern and cabling procedure, in particular on the cabling compaction at the various cabling stages. Because of the importance in the control of AC loss and the implications for stability, the interstrand conductance is the subject of an intense experimental study for various cable types and configurations. Finally, the strand self and mutual inductances are known to affect the dynamic response of a cable to current and field transients. In spite of this, especially when compared to the effort in the characterization of the resistive properties of cables, cable inductances are not intensively studied. Part of this could be due to the fact that a measurement of the strand self inductance and the interstrand mutual inductances is not easy. A measure of inductance in a cable demands access to single strands, which is not practical in the case of large cables. A frequency analysis can be used to discriminate the inductive effects from the resistive ones and thus infer the strand inductances from the measured impedances [7]. This method has limited accuracy. Finally, inductance is an integral property of the cable geometry, so that the inductance of a cable wound in a coil is in general different from that of a straight cable sample. The results thus depend on the measurement conditions.

Based on the above arguments, we have developed a geometric model of a cable that is suitable for the calculation of the strand inductances. In addition, the geometric model can be used for the estimation of the interstrand contact pattern and hence to estimate the expected interstrand conductance, assuming that the conductance of a single, isolated contact is known. In this paper we describe the main features of the geometric model and the calculation procedures for the inductances and interstrand conductances. We show that the inductance calculation is sound and stable by comparison to another numerical method, based on a different approach. Finally we present some calculation results for relevant examples of a subcable of a cable-in-conduit conductor (CICC) of the ITER class [8], and for a Rutherford cable as used in the LHC [9]. The examples are used to show general trends in the electrical parameters of cables as a function of cabling pattern, size and compaction.

Cable geometry

The cable geometry is generated first in a reference *x-y* plane, located at the origin of the cable, and is then *extruded* in the third dimension *z* taking into account the cable twist-pitches and cabling direction, reproducing the physical cabling process in a virtual analog. The starting components are strands of round shape, cabled in an arbitrary number and composition (e.g., mixing superconducting and pure stabilizer strands of different diameter) to form a sub-stage of round shape and with a given outer diameter. Cabling around a core has been implemented also to model, for example, cabling patterns of the type of 6-around-1, or cabling around a central hollow space. Figure 1 shows the general sub-stage assemblies that have been considered.

This assembly process can be repeated recursively up to the last level of cabling. The cable is then formed by arranging an arbitrary assembly of elements in a final shape that can be chosen among a round (as is the case for sub-cables), a rectangular or a keystoned

geometry. This makes it possible to generate geometries ranging from round, square and rectangular CICC's, to CICC's with central cooling hole, or flat and keystoned Rutherford cables. Some examples of the geometry generated are reported later.

Once the geometry is generated in the reference plane, the centres of the building components are known in polar coordinates and are located at radius R_i^l and angle $\theta_i^l(0)$ where the superscript l is the identifier of the cabling stage and the subscript i is the index of the element in the cabling stage. A schematic representation of the coordinate identification in the reference plane for a simple case of a 3x4 cabling pattern is shown in Fig. 2.

For round cables, the coordinates of the centerline of the strands are computed as a function of z in 3-D coordinates space as follows:

$$\begin{aligned} x_i &= \sum_{j=1}^{N} R_i^j \cos\left(q_i^j \pm 2p \frac{z}{L_p^j} \right) \\ y_i &= \sum_{j=1}^{N} R_i^j \sin\left(q_i^j \pm 2p \frac{z}{L_p^j} \right) \end{aligned} \tag{1}$$

where L_p^j is the twist pitch of the cabling stage j. The sign + or – in the trigonometric functions of Eq. (1) are selected depending on the cabling pattern ("S" or "Z"). This calculation neglects the effect of the following cabling sequences on the curvilinear coordinate along the strand. We assume that this effect introduces a small error compared to other possible error sources. In the case of rectangular or keystoned cable shapes, the strands are first placed uniformly on a circle as implied by Eq. (1), as it is the case on a real winding machine before passing through the turcks head and compaction dies. This circle is then transformed in the desired shape by an isoparametric transformation between the *physical* plane (x,y) and a *parent* plane (x,h), where the cable is a square with corners placed at unit coordinates [10]. The transformation is shown schematically in Fig. 3 for the case of a cable of width w formed of strands of diameter d.

We have chosen to discretize the strands in 3-D using isoparametric, 8-nodes brick elements [10]. The discretization is performed automatically, using the coordinates of the centers of the strands to define the line along which the isoparametric bricks are created. The cross-sectional dimensions of the brick elements in the plane normal to the z direction are set so that the strand cross section is maintained. The number of subdivision N_z in z direction is chosen large enough to lead to accurate numerical results, as discussed later. Figure 4 shows a detail of the geometry discretization in 3-D coordinates generated for the cross section reported in Fig. 2. At present the model cannot avoid strand interference and inter-penetration of the isoparametric bricks, but we are experimenting methods that could resolve interference either imposing geometrical constraints or simplified mechanical constraints.

Inductance calculation

For the calculation of the self and mutual inductance of the strands we use the standard definition of the inductance coefficient L_{ij} between two strands i and j of volume V_i and V_j, whose internal points **P** and **Q** are located at a distance $\mathbf{r}_{PQ}$. The strands have current densities $\mathbf{J}_i$ and $\mathbf{J}_j$ respectively. We define two vectors $\mathbf{j}_i$ and $\mathbf{j}_j$ with directions identical to those of the current densities $\mathbf{J}_i$ and $\mathbf{J}_j$, and module equal to the inverse of the cross section normal to the current flow. With this definition, $\mathbf{j}_i$ and $\mathbf{j}_j$ are the current densities that correspond to unit current in the two strands. The inductance is then given by:

$$L_{ij} = \frac{m_0}{4p} \int_{Vi} \int_{Vj} \frac{\mathbf{j}_i \bullet \mathbf{j}_j}{\left|\mathbf{r}_{PQ}\right|} dV_j dV_i \qquad (2).$$

Introducing the magnetic vector potential $\mathbf{A}_j$ generated by the current density of strength $\mathbf{j}_j$ in the strand j:

$$\mathbf{A}_j = \frac{m_0}{4p} \int_{Vj} \frac{\mathbf{j}_j}{\left|\mathbf{r}_{PQ}\right|} dV_j \qquad (3)$$

we can transform the definition of the inductance coefficient as follows:

$$L_{ij} = \int_{Vi} \mathbf{j}_i \bullet \mathbf{A}_j dV_i \qquad (4).$$

In the above form, the inductance calculation can therefore be reduced to the volume integral in strand i of the scalar product of the current density versor $\mathbf{j}_i$ and the vector potential $\mathbf{A}_j$ generated by a current density of strength $\mathbf{j}_j$ in the strand j. This is the most convenient form for numerical integration.

In practice, the integral of the scalar quantity, the product $\mathbf{j}_i \bullet \mathbf{A}_j$, over the volume V_i of strand i is broken into the sum of the integrals over the N_z isoparametric elements of volume V_{Nz} that are used to discretize the strand:

$$L_{ij} = \int_{Vi} \mathbf{j}_i \bullet \mathbf{A}_j dV_i = \sum_{Nz} \int_{V_{Nz}} \mathbf{j}_i \bullet \mathbf{A}_j dV_{Nz} \qquad (5).$$

To perform the volume integration in each element of strand i, we need the value of the vector potential generated at an arbitrary point by the elements belonging to strand j. For this calculation we use the analytic expressions established in [11] in the case of an arbitrary isoparametric element carrying a uniform current density. The integral over the volume V_{Ni} is then performed numerically using Gauss quadrature [10], as detailed in [12].

Strand contact pattern and interstrand conductance

Starting from a discretized cable geometry it is possible to use the distance between strands to identify the interstrand contacts [13, 14, 15]. An interstrand contact between strands i and j is defined as the point where the distance d_{ij} between the centers of the strands is smaller than the sum of the strand radii. The contact condition is therefore:

$$d_{ij} \leq \frac{d_i + d_j}{2} \tag{6}$$

where d_i and d_j are the strand diameters. This condition must be verified continuously along the cable, as a function of the z coordinate, to detect one or more contacts. We have chosen to verify it at all isoparametric elements, on the points z_{up} and z_{low} corresponding to the two faces parallel to the x-y plane. By doing this, we have defined two possible types of contacts between strands, as shown schematically in Fig. 5. The first type is a *line* contact, taking place when both points at z_{up} and z_{low} satisfy the condition Eq. (6). This type of contact is best characterised using the distributed conductance g_{line} defined for a unit length of contact (i.e., with dimensions of [S/m]). The second type is the *cross* contact, defined when only one of the two points satisfies the contact condition Eq. (6). This contact is characterised electrically by the contact conductance G_{cross}. Once the topology of all contacts is found, it is possible to compute the interstrand conductance per unit length between the two strands:

$$g_{ij} = \frac{1}{L}\left(N_{cross} G_{cross} + N_{line} g_{line} \frac{L}{N_z} \right) \tag{7}$$

where N_{cross} and N_{line} are the total number of cross and line contacts respectively, L is the total length of cable modelled and analysed and N_z is the number of subdivisions in z direction, so that L/N_z is the length of a single isoparametric element in z direction.

Since the contact condition (6) is verified at a finite number of points, the contact topology and, in particular, the number of contacts found depend on the level of discretization. This can be obviated using a sufficiently large number of subdivisions N_z and providing a tolerance range for the contact condition.

Model validation

As we discussed in the introduction, a direct verification of the electrical coupling parameters is not easy. Some attempt at validating models similar to that described here have been reported in the literature [15] with encouraging results. Here we focus mainly on inductances, and we validate our calculations comparing them to the results of an independent model that uses analytical strand trajectories to solve the 6-D integral of Eq. (2) [16, 17]. The cases that have been selected for a comparison are two:

- three lengths, 100, 200 and 540 mm, of the first two stages of a cable with characteristics similar to the ITER-CS1 cable [8], reported in Tab. 1. Note that the outer diameter chosen for the two stages is identical to the diameter of the envelope of the outer strand surfaces in the two cabling stages, as shown in Fig. 2. The diameter of a compacted cable is generally smaller than the values taken in Tab. 1;
- a single twist pitch of a keystoned, Rutherford cable with the typical dimensions of the inner cable used for the LHC dipoles [9], and characteristics reported in Tab. 2;

The results of the comparison for the ITER-CS1 subcables is shown in Fig. 6. The agreement is excellent for the triplet, with a relatively simple geometry, and is satisfactory for the 3x4 subcable. The results shown in Fig. 6 have been obtained with a number of z subdivisions sufficient to insure convergence of the numerical integration. Typically 10 subdivisions per twist pitch are necessary to describe accurately the twisted strands geometry. We attribute the small residual differences observed in this case to variations of the geometry used in the integration and the residual error at the specified convergence tolerance of 5 %. The results for the LHC inner cable are shown in Fig. 7, and display a very good agreement between the two calculation methods. Based on these results, we have confidence in the quality and accuracy of the calculation method presented.

Applications

We have used the model described above to study two parameters that are fundamental in determining the maximum intensity and the longest time constant of induced currents in superconducting cables. The first parameter is the *return line inductance* per unit length l_{ij}, defined for any couple of strands i and j as:

$$l_{ij} = l_{ii} + l_{jj} - 2l_{ij} \tag{8}.$$

The second parameter of relevance is the *total return conductance* per unit length g_i defined for any strand i as:

$$g_i = \sum_{j=1}^{N_{strands}} g_{ij} \tag{9}$$

which corresponds to the conductance per unit length experienced by a current flowing in strand i and returning in the other strands. It can be shown [18, 19] that the amplitude of the current imbalance induced in a multi-strand cable by external sources such as localised or distributed voltages is proportional to the return conductance g_i, while the time constant of the evolution of the imbalance is proportional to the product of the return inductance and conductance $l_{ij}\, g_i$.

In the case of the LHC inner cable the spectrum of return line inductances is shown in Fig. 8. The return line inductances are relatively small for adjacent strands, 0.3 μH/m, and grow to a maximum of 1 μH/m for strands opposite in the cable. The implication is that the time constants of current distribution span a spectrum with the same width. The case for a multi-stage twisted cable is more interesting. Taking the first three stages of the ITER-CS1 cable as an example, the return line inductance for the first stage (triplet) is small, approximately 0.4 μH/m, similar to adjacent strands in the case of a Rutherford cable. As the cable becomes larger and more complex, the spectrum shows a steady rise, reaching values in excess of 1 μH/m for the 3x4x4 subcable as shown in Fig. 9. Clearly, the return inductances (and the corresponding time constants) will be significantly larger in the final cable stage.

An interesting feature of the model is that it allows the generation of cables geometries with different final diameter, thus simulating the effect of cable compaction. We have studied the effect of cable compaction on the return inductance and conductance of the second stage (3x4) of the ITER-CS1 cable. The final diameter of the cable has been reduced scaling it by a factor in the range of 0.85 (15 % compaction) to 1 (0 % compaction) without modifying the strands, and the corresponding inductance and conductance matrices have been used to determine the spectrum of l_{ij} and g_i. The results of this study are shown in Figs. 10 and 11, where we have plotted the effect of cable compaction on the average, minimum and maximum of the spectra of l_{ij} and g_i. The effect on the return inductance (Fig. 10) is marginal and smooth, resulting in a change of 15 % over the whole range of compaction tested. In contrast, as expected, the estimated effect on the return conductance is large and shows a threshold at a cable compaction of 5 %. For compaction below 5 %, the return conductance is governed by line contacts among the strands in a triplet. Above 5 %, the strands of different triplets come in contact and the return conductance grows sharply, reaching saturation at high enough compaction. The absolute magnitude of this effect depends on the values taken for the line and cross conductances, see Tab. 1. Although the details of interstrand conductance are much more complex than the simplistic approach discussed here, it is interesting to note that a simple model can still give useful quantitative indications on trends.

Conclusions

The model described in this paper provides useful information for the characterization of the electrical properties of a multi-strand superconducting cable. We have verified the inductance calculation through comparison to a semi-analytical model, developed independently, achieving good agrement between the two calculations. Further validation tests will include a mandatory comparison to experimental results.

The flexibility of our general approach is an advantage when dealing with multi-stage cables, for which an analytical description of the cable geometry is not feasible. The contact model, although rudimentary in its principle, has an inherent level of complexity associated with the geometry description that makes its detailed interpretation already difficult. However, it appears to produce physically consistent trends and definitely demands a more precise quantitative validation.

The examples discussed demonstrate that the electrical characterization of a multi-strand superconducting cable is a complex task, involving a multitude of parameters. The consequences is that simple estimations can be wrong, in some cases by orders of magnitude, leading to wrong assumptions on the transient and steady state electrical response of a cable. We believe that the approach described here is a step in the direction of an improved understanding through enhanced knowledge of key parameters such as interstrand inductance and conductance.

References

[1] B. Turck, *Influence of a transverse conductance on current sharing in a two-layer superconducting cable*, *Cryogenics*, **24**, 448-454, 1974.

[2] G. Ries, *Stability in superconducting multistrand cables*, Cryogenics, **20**, 513-519, 1980.

[3] L. Krempasky, C. Schmidt, *Theory of "supercurrents" and their influence on field quality and stability of superconducting magnets*, Jour. Appl. Phys., **78** (9), 5800-5810, 1995.

[4] A. P. Verweij, *Electrodynamics of Superconducting cables in Accelerator Magnets*, Ph.D. Thesis, University of Twente, Enschede, Netherlands, 1995.

[5] N. Amemiya, *Overview of Current Distribution and Re-distribution in Superconducting Cables and their Influence on Stability*, Cryogenics, **38**, 545-550, 1998.

[6] A. Akhmetov, L. Bottura, M. Breschi, *A Continuum Model for Current Distribution in Rutherford Cables*, IEEE Trans. Appl. Sup., **11**, 2138-2141, 2001.

[7] M. Ono, Y. Wachi, T. Hamajima, M. Yamaguchi, Y. Sawada, K. Yamamoto, T. Fujioka, *Estimation Method of Stability for the Multi-strand Superconducting Cables under Partial Current Distribution*, IEEE Trans. Appl. Sup., **5**(2), 564-567, 1995.

[8] N. Mitchell, et al., *Conductor Development for the ITER Magnets*, Proc. Of the 15th Int. Mag. Tech. Conf. Beijing, Science Press, 347-352, 1998.

[9] J.D. Adam, T. Boutboul, G. Cavallari, Z. Charifoulline, C.H. Denarie, S. Le Naour, D.F. Leroy, L.R. Oberli, D. Richter, A.P. Verweij, R. Wolf, *Status of the LHC Superconducting Cable Mass Production*, IEEE Trans. Appl. Sup., **12**(1), 1056-1062, 2002.

[10] O.C. Zienkiewicz, *The Finite Element Method*, 4th Edition, McGraw Hill, 1991

[11] L. Bottura, *Analytical Calculation of Vector Potential in an Isoparametric Brick*, CryoSoft Internal Note CRYO/97/003, 1997.

[12] L. Bottura, *Inductance Calculation for Conductors of Arbitrary Shape*, CryoSoft Internal Note CRYO/02/028, 2002.

[13] K. Seo, K. Fukuhara, M. Hasegawa, *Analyses for Inter-strand Coupling Loss in Multi-strand Sueprconducting Cable with Distributed Contact Resistance Between Strands*, Cryogenics, **41**, 131-137, 2001.

[14] K. Seo, K. Fukuhara, M. Hasegawa, *Relation Between Inter-sub-cable Contact Resistance and Coupling Loss in Multiple-stage Stranded Cable*, IEEE Trans. Appl. Sup., **12**(1), 1635-1638, 2002.

[15] F. Bellina, D. Boso, B.A. Schrefler, G. Zavarise, *Modelling a Multistrand SC Cable with an Electrical Lumped Network*, IEEE Trans. Appl. Sup., **12**(1), 1408-1412, 2002.

[16] M. Breschi, *Current Distribution in Multistrand Superconducting Cables*, Ph.D. Thesis, University of Bologna, Italy.

[17] M Fabbri, P.L. Ribani, *A priori error bounds on potentials, fields, and energies evaluated with a modified kernel*, IEEE Transactions on Magnetics, **37**, 4 (2) , pp. 2970 –2976, 2001.

[18] L. Bottura, M. Breschi, M. Fabbri, *Analytical Solution for the Current Distribution in Multistrand Superconducting Cables*, paper accepted for publication in J. Appl. Phys., 2002.

[19] L. Bottura, M. Breschi, M. Fabbri, *Analytical Calculation of Current Distribution in Multistrand Superconducting Cables*, paper presented at 2002 Appl. Sup. Conf., Houston, to appear in IEEE Trans. Appl. Sup. 2003.

Strand diameter	(mm)	0.81
Cabling pattern		3x4x4
1^{st} stage (triplet)		
outer diameter	(mm)	1.75
twist pitch	(mm)	25
2^{nd} stage (quadruplet)		
outer diameter	(mm)	4.21
twist pitch	(mm)	54
3^{3d} stage (quadruplet)		
outer diameter	(mm)	10.17
twist pitch	(mm)	95
G_{cross}	(MS)	1
g_{line}	(MS/m)	20

Table 1. Geometrical and electrical characteristics used for the calculation of the electrical parameters of the first cabling stages of the ITER-CS1 cable.

Strand diameter	(mm)	1.07
Number of strands	(-)	28
Width	(mm)	15.1
Inner thickness	(mm)	1.74
Outer thickness	(mm)	2.06
Twist pitch	(mm)	115

Table 2. Geometrical characteristics used for the calculation of the electrical parameters of the inner cable of the LHC dipoles.

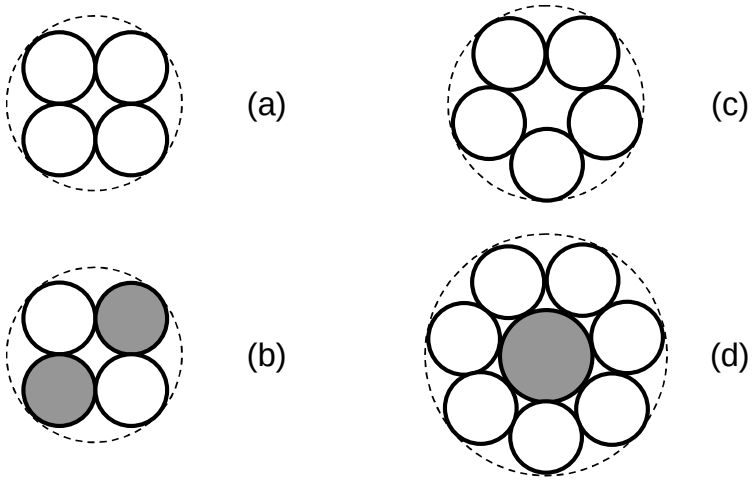

Figure 1. Cabling patterns considered for a sub-cable stage: (a) a n-plet of superconducting strands, (b) an hybrid of superconducting strands and pure stabilizer strands, (c) a hollow cable and (d) cable around a core with different diameter and material (e.g., pure stabilizer).

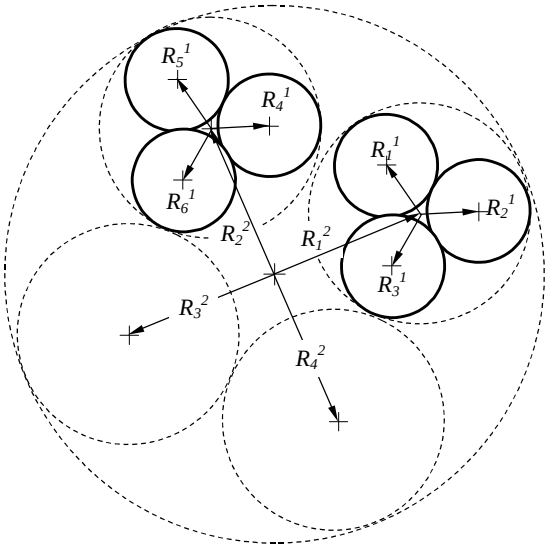

Figure 2. Definition of the polar coordinates of the sub-elements of a 3x4x4 cable in the reference plane. Only two triplets (stage 1) are shown for clarity.

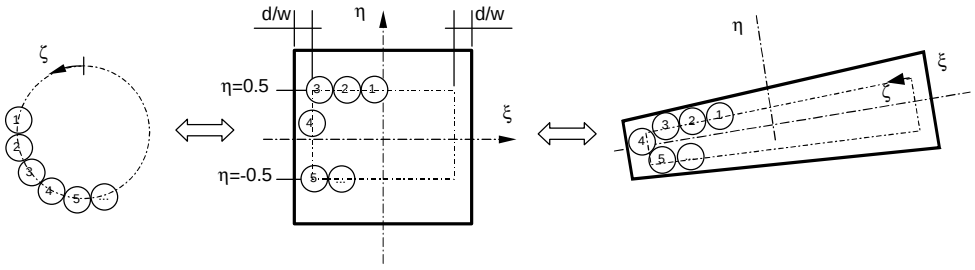

Figure 3. Principle for randomized meshing of a cable. The first strand is placed randomly on the ζ circle, the following strands are equispaced. This distribution is then mapped first in the parent plane and afterwards in the physical plane.

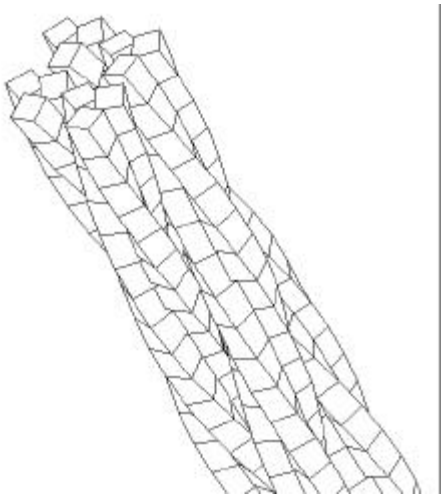

Figure 4. Detail of the geometry generated for a 3x4 cable with the cross section shown in Fig. 2. Note the inversion in the twisting direction between first and second stage.

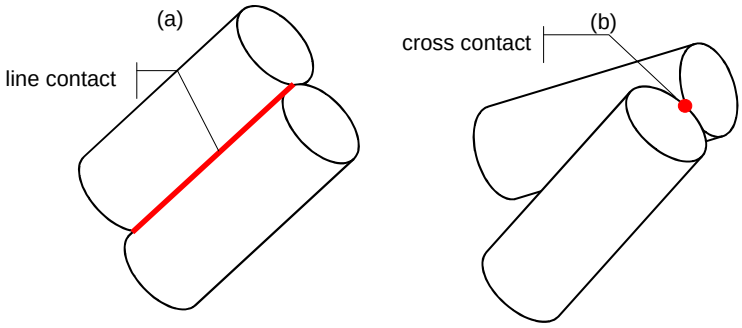

Figure 5. Definition of a line contact (a) and a cross contact (b).

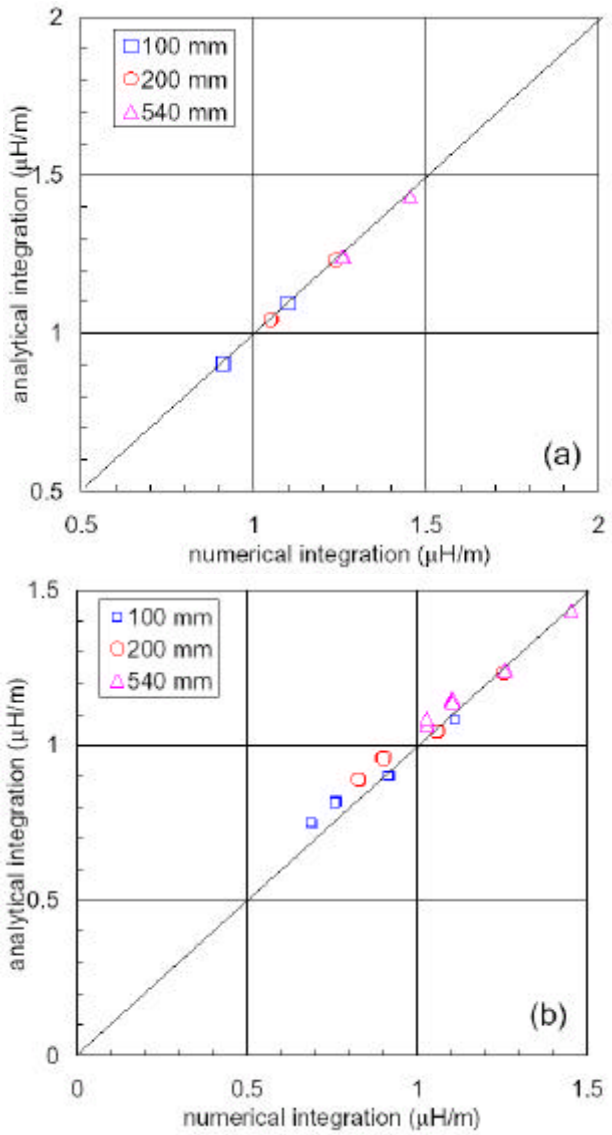

Figure 6. Comparison of computed strand self and mutual inductances per unit length in the case of an ITER-CS1 triplet (a) and for a 3x4 cable substage (b). The results of the numerical procedure described in this paper (plotted on the x axis) are compared to the results obtained by direct 6-D integration of the inductance of round conductors with analytical centerline (plotted on the y axis). The calculations have been performed for different cable lengths.

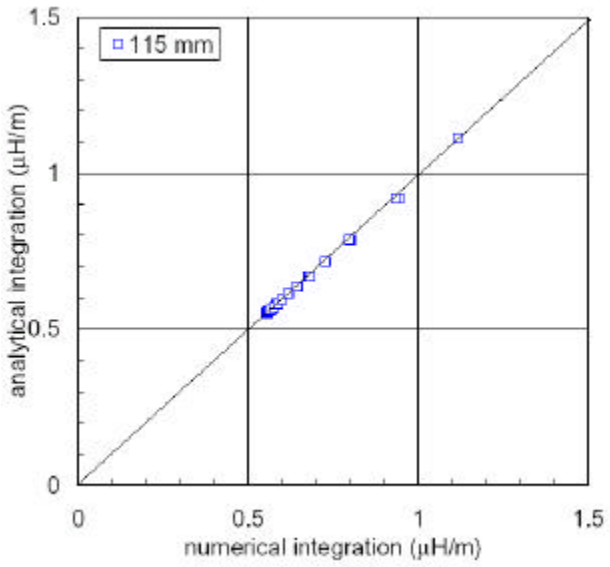

Figure 7. Comparison of the calculation of self and mutual inductances per unit length in the case of a Rutherford cable for the inner layer of an LHC dipole, computed for a cable with a length of 115 mm (one twist pitch).

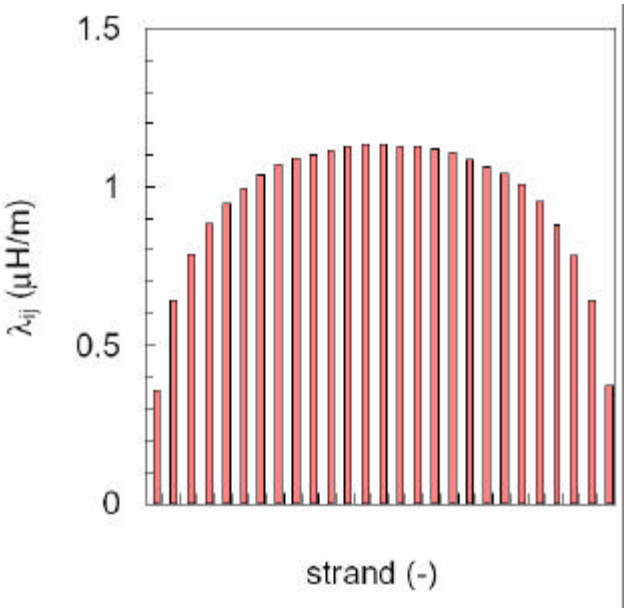

Figure 8. Spectrum of the return line inductances computed for the LHC inner cable.

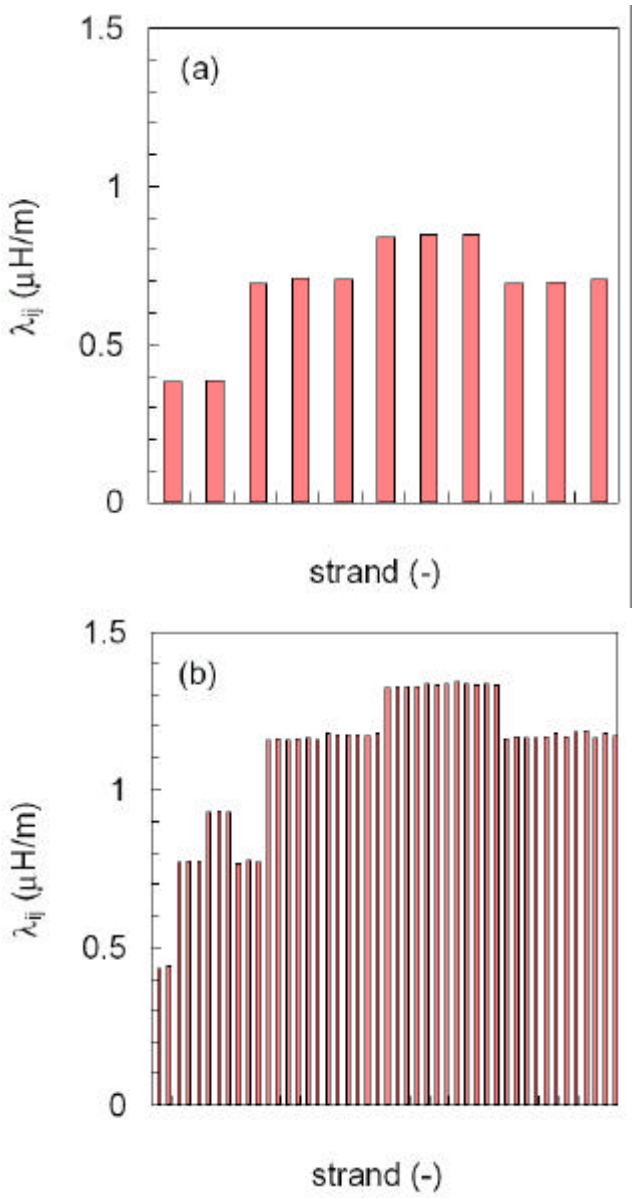

Figure 9. Spectrum of the return line inductances computed 3x4 (a) and the 3x4x4 (b) cabling stages of the ITER-CS1 cable. The return line inductance grows significantly as the subcable increases its size.

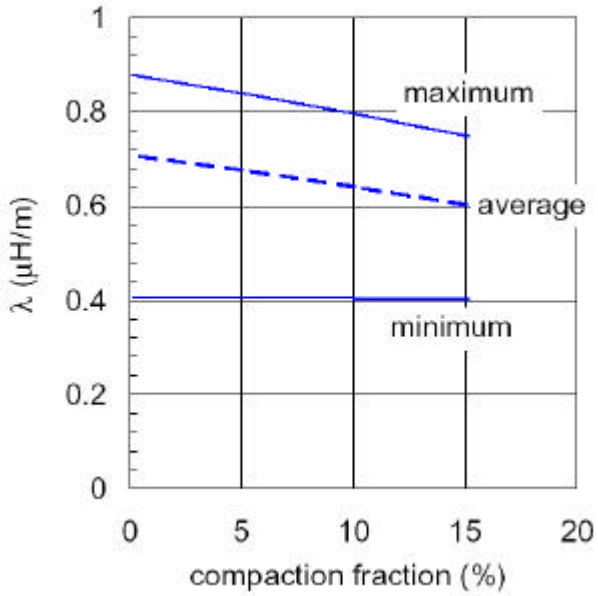

Figure 10. Estimate of the effect of cable compaction on the average, minimum and maximum return line inductance in a 3x4 subcable of the ITER-CS1 cable.

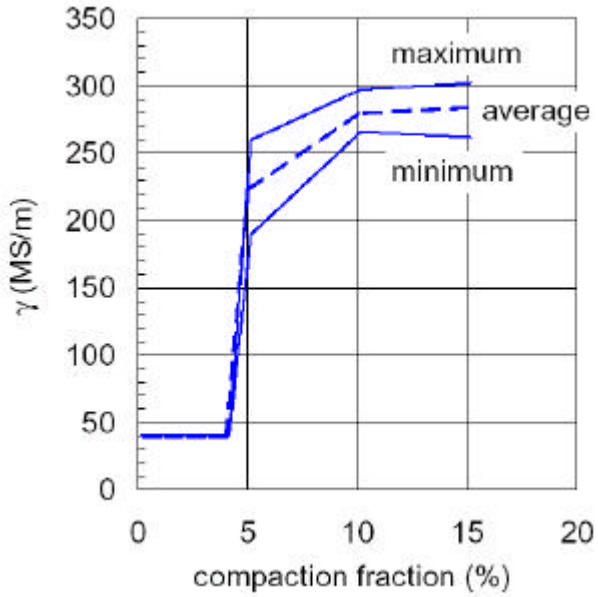

Figure 11. Estimate of the effect of cable compaction on the average, minimum and maximum total interstrand conductance in a 3x4 subcable of the ITER-CS1 cable.